SECOND EUROPEAN CONFERENCE ON EARTHQUAKE ENGINEERING
AND SEISMOLOGY, ISTANBUL AUG. 25-29, 2014

NUMERICAL STUDY ON FLEXURE-SHEAR-CRITICAL RC COLUMN

Wencong LI[1] and Oh-Sung KWON[2]

ABSTRACT

Predicting the inelastic hysteretic behaviour of shear-critical or flexure-shear-critical RC columns is still a difficult task in the field of structural engineering. In this paper, two numerical modelling methods for a flexure-shear-critical RC column are evaluated. In one of the methods, the fiber element in OpenSees is used together with lumped shear spring element and shear limit curve. In the other method, continuum element in VecTor2 which is based on the Modified Compression Field Theory and the Disturbed Stress Field Model for FEM is utilized. The model with fiber element in OpenSees is computationally efficient but requires empirical approach to model the shear deformation and failure. The model in VecTor2 is computationally more demanding. The VecTor2 model, however, can be applied to general geometrical configuration and rebar layout.

INTRODUCTION

It is well known that reinforced concrete columns with light or widely spaced transverse reinforcement are vulnerable to shear failure. For the evaluation of the cyclic behaviour of shear-critical RC columns, experimental test can be the most reliable source. However, in many practical problems, it is very difficult and costly to test actual specimens. Instead, numerical models are used to capture the nonlinear behaviour of structural elements. Even though there have been many years of experimental and analytical investigations, replicating the hysteretic behaviour of flexure-shear-critical RC column is still a very challenging task. In this paper, two numerical modelling methods for a flexure-shear-critical RC column tested by Li and Esaki (2010) are evaluated. In one of the methods, the fiber element in OpenSees (Mazzoni et al., 2007) with lumped shear spring at the end is used. In the other method, continuum element in VecTor2 (Vecchio et al., 2004) is utilized. The responses from both numerical models are compared with the experimental results in (Li and Esaki, 2010).

SPECIMEN

A RC specimen with poor transverse reinforcement is the object of the numerical analysis in this study. The dimensions and reinforcement properties of the specimen are illustrated in Fig. 1. The experimental parameters of the specimen are summarized in Table 1. The mechanical properties of reinforcement bars are listed in Table 2. The specimen has sectional dimension of 200 mm x 200 mm and height of 800 mm. The shear span to depth ratio of the column is 2.0. Four D13 reinforcement bars are used as longitudinal reinforcements with longitudinal reinforcement ratio, p_g, of 1.33%. Transverse reinforcement bars consist of 4ϕ bars spaced at 155 mm interval (transverse reinforcement ratio, p_w= 0.08%). Cyclic lateral displacements are applied to the specimen without applying axial load.

[1] Assistant Professor, Fukuoka University, Fukuoka, Japan, liwencong@fukuoka-u.ac.jp
[2] Assistant Professor, University of Toronto, Toronto, Canada, os.kwon@utoronto.ca

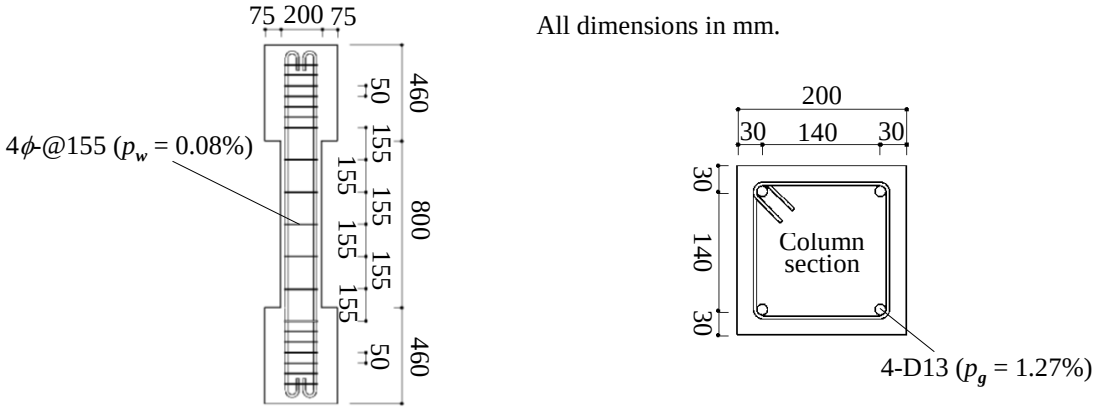

Figure 1. Dimensions and reinforcement properties

Table 1. Experimental parameters

Experimental parameters	$M/(Q \cdot D)$=2.0, Concrete compressive strength σ_B = 26.7MPa, Axial force ratio $N/(b \cdot D \cdot \sigma_B)$ = 0, Rebar : 4-D13 (p_g = 1.27%), Hoop : 4ϕ-@155 (p_w = 0.08%).

Table 2. Mechanical properties of reinforcement

Reinforcement		a (cm^2)	f_y (MPa)	ε_y (%)	E_S (GPa)
Longitudinal reinforcement	D13	1.27	346	0.19	187
Transverse reinforcement	4ϕ	0.13	199	0.1	197

Note: a = cross-sectional area, f_y = yield strength of steel, ε_y = yield strain of steel, E_S = modulus of elasticity.

EXPERIMENTAL RESULTS

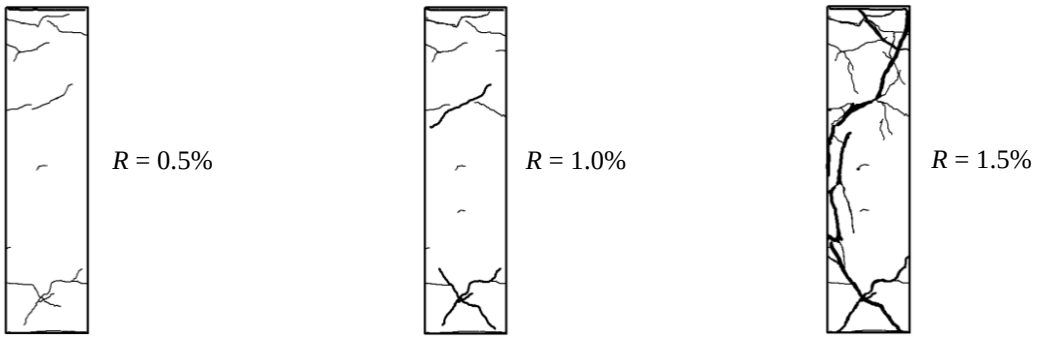

Figure 2. Observed crack patterns of column in depth side

Crack patterns of the specimen at the drift angle, R, of 0.5%, 1.0% and 1.5% are illustrated in Fig. 2. The relationship between the experimental lateral force, Q, and the drift angle, R, of the specimen is shown in Fig. 3. The relationship between the average vertical strain ε_v along the column axis and the drift angle, R, of this specimen is also shown in this Figure. In the Q-R curve, the dotted lines are the calculated flexural strength of column V_f based on the standard published by Architectural Institute of Japan (1990), and the solid lines are calculated shear strength of column V_u proposed by Sezen (2002). The model divides the shear strength into two terms: the shear carried by the concrete, V_c; and the shear carried by the reinforcement through a 45° truss model, V_s. The V_u is defined as follows:

$$V_u = k(V_c + V_s) = k\frac{6\sqrt{f_c'}}{a/d}\sqrt{1+\frac{N}{6A_g\sqrt{f_c'}}}0.8A_g + k\frac{A_s \cdot f_{yw} \cdot d}{s} \quad \text{(psi)} \qquad (1)$$

where, f_c' is the concrete compressive strength, N is the axial load on the column, A_g is the gross concrete area, a is a distance from maximum moment to inflection point, d is the effective depth, A_s is the area of the transverse reinforcement, f_{yw} is the yield strength of the transverse reinforcement, and s is the spacing of the transverse reinforcement. The coefficient k defines the degradation of shear strength with increasing displacement ductility, μ_δ, as shown in Fig. 4.

When the drift angle R was approximately 0.5%, flexural cracks were observed at both ends of the column, and then oblique cracks developed. Rebars around critical sections of the column yielded when the drift ratio approached 1.0%, and the experimental lateral capacity of 41.2kN was measured which exceeded the calculated flexural strength of column V_f. The width of oblique cracks increased subsequently. Because of the poor transverse reinforcement and degradation of shear strength with increasing displacement ductility, the column failed in shear during the second load cycle of R = 1.5% (see Fig. 3). Because no axial force was applied to the column, the variation of average vertical strain ε_v of this specimen was not significant when shear failure occurred.

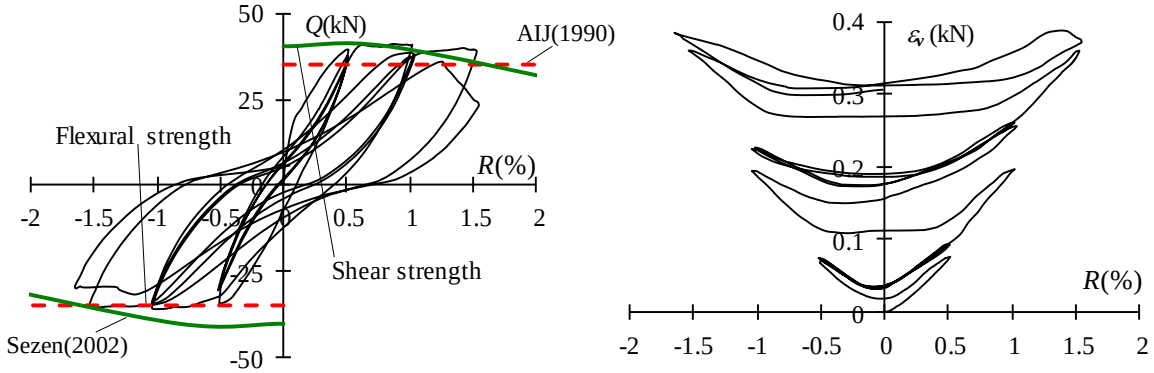

Figure 3. Measured Q-R and ε_v-R relationships

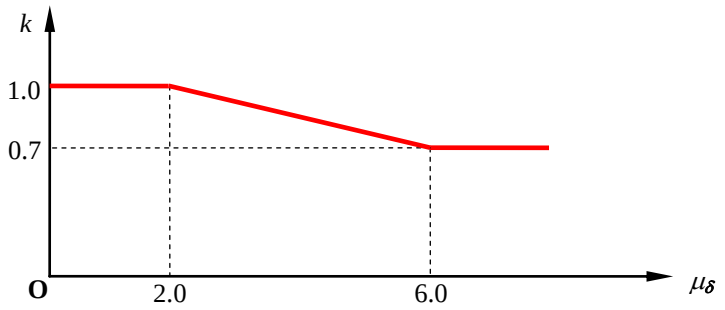

Figure 4. Variation of degradation coefficient k with displacement ductility μ_δ

NUMERICAL MODELLING WITH OPENSEES

This section describes a nonlinear numerical study on the tested specimen based on OpenSees (Mazzoni et al., 2010). OpenSees is a software framework for simulating the seismic response of structural and geotechnical systems. It has been developed as the computational platform for research in performance-based earthquake engineering at the Pacific Earthquake Engineering Research Center.

Fig. 5 illustrates the numerical element of the specimen in OpenSees. The numerical element consists of a two-dimensional nonlinear beam-column with fiber sections located at the integration points. Each section is subdivided into a number of fibers where each fiber is under uniaxial state of stress. The specimen is modelled with three nodes and each node has three degrees-of-freedom. Node

1 is fully fixed, and node 3 is constrained on rotation only. In order to capture shear strength degradation, a shear spring is modelled between nodes 2 and 3 utilizing zero-length element (see Fig. 5). The shear spring is defined with the limit state material and the shear limit curve based on the work of Elwood and Moehle (2003). Note that the vertical translation and rotational degrees of freedoms (DOFs) of node 2 are constrained with the DOFs of node 3.

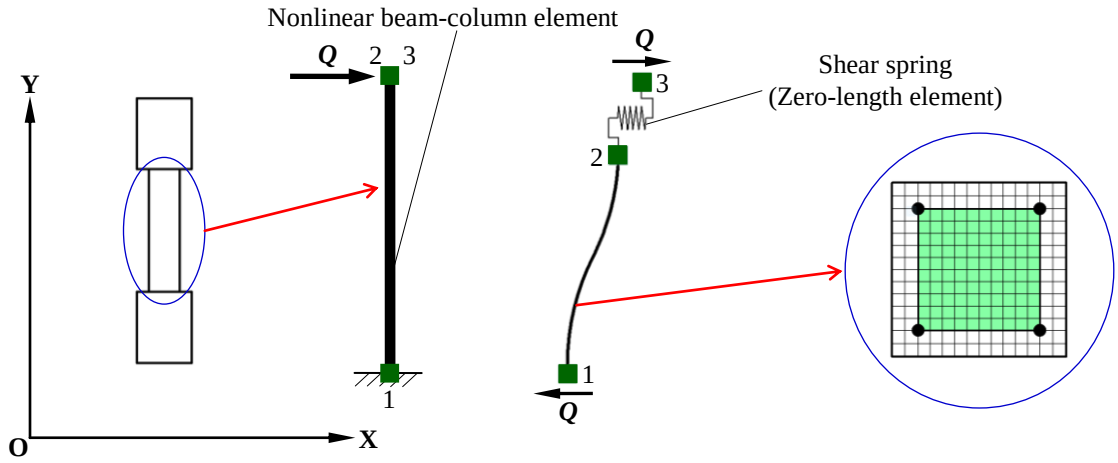

Figure 5. Numerical element in OpenSees

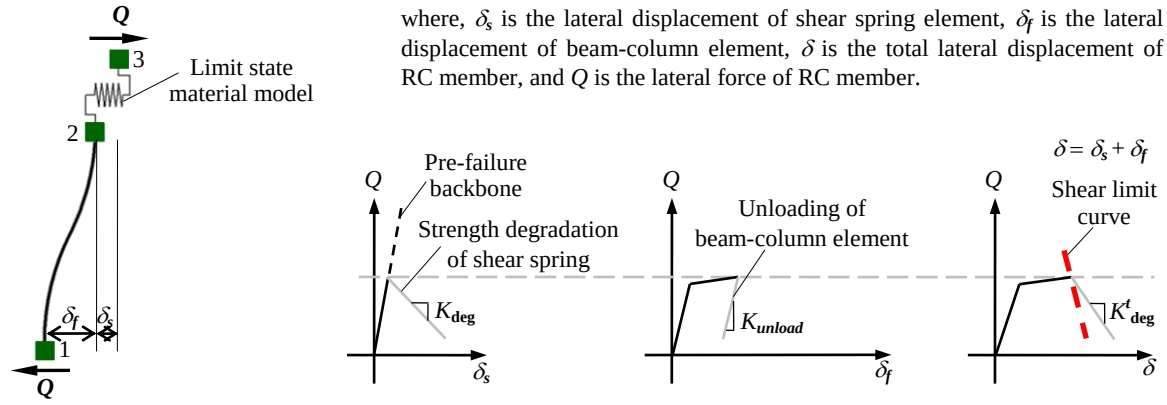

a) Shear spring in series model b) Shear spring response c) Beam-Column response d) Total response

Figure 6. Shear spring in series model utilizing limit state uniaxial material model and lateral force-displacement response at shear failure

Fig. 6 illustrates the shear spring in series model utilizing limit state uniaxial material model and the response of the column for monotonically increasing total displacements at shear failure. The total lateral displacement of RC member, δ, becomes the superposition of the lateral displacement of shear spring element, δ_s, and the lateral displacement of beam-column element, δ_f. The limit state material model is used to define the force-deformation relationship of the shear spring in series with a beam-column element. The uniaxial material model monitors the response of the beam-column element to detect the onset of shear failure. As shown in Fig. 6, the limit curve is defined based on the column shear, Q, and the displacement, δ (or the drift angle, R). If the column is vulnerable to shear failure after flexural yielding, then the drift capacity model proposed by Elwood and Moehle (2005) is used to define the limit curve. And the drift ratio at shear failure, R_s, is estimated as follows:

$$R_S = \frac{3}{100} + 4p_w - \frac{1}{40}\frac{\nu}{\sqrt{f_c}} - \frac{1}{40}\frac{P}{A_g' \cdot f_c} \geq \frac{1}{100} \quad \text{(MPa)} \qquad (2)$$

where, p_w is the transverse reinforcement ratio, ν is the nominal shear stress (in MPa), f_c is the concrete compressive strength (in MPa and positive for compression), P is the axial load on the column, and A_g' is the gross cross-sectional area.

The pre-failure backbone for the limit state material model is selected as linear with a steep slope equal to the shear stiffness of an uncracked column. Note that by defining the limit curve based on the total displacement, the shear deformations are included in the displacements monitored by the uniaxial material model, and shear failure is based on the sum of the flexure and shear deformations.

When the total response of RC member hits the shear limit curve for the first time, the shear failure is detected, and the backbone of the shear spring is redefined, as shown in Fig. 6, to include the degrading slope, K_{deg}.

After shear failure is detected, the response follows the grey line as shown in Fig. 6. Additional lateral demands will result in strength degradation of the shear spring and an increase in the shear deformations, accompanied by unloading of the beam-column element, and therefore, a slight reduction in the flexural deformations.

When shear failure is detected, based on the intersection of the total response and the shear limit curve, the degrading slope for the total response, K^t_{deg}, is estimated as follows:

$$K^t{}_{\deg} = \frac{V_u}{\left(\Delta_a - \Delta_s\right)} \tag{3}$$

where, V_u is the ultimate shear capacity of the RC column, Δ_s is the calculated displacement at shear failure, Δ_a is the calculated displacement at axial failure. Since the shear spring element and beam-column element are in series, the total flexibility is equal to the sum of the flexibilities of the shear spring and the beam-column element. Hence, K_{deg} can be determined as follows:

$$K_{\deg} = \left(\frac{1}{K^t{}_{\deg}} - \frac{1}{K_{unload}} \right)^{-1} \tag{4}$$

where, K_{unload} is the unloading stiffness of the beam-column element. It depends on the boundary conditions of the column. In this study, K_{unload} is estimated as follows:

$$K_{unload} = \frac{12E \cdot I_{eff}}{L^3} \tag{5}$$

where, $E \cdot I_{eff}$ is the effective flexural stiffness of RC column, and L is the height of RC column. Note that K_{unload} must be provided as an input parameter for the limit state material model.

The axial capacity model by Elwood and Moehle (Elwood and Moehle, 2003) suggests that the drift at axial failure, R_a, is inversely proportional to the axial load supported by the column and directly proportional to the amount of transverse reinforcement. The R_a can be calculated as following Eq. (6).

$$R_a = \frac{\Delta_a}{L} = \frac{4}{100} \frac{1 + \left(\tan\theta\right)^2}{\tan\theta + P\left(\frac{s}{A_s \cdot f_{yw} \cdot d_c \cdot \tan\theta} \right)} \quad \text{(MPa) or (psi)} \tag{6}$$

where, d_c is the depth of the column core from center line to center line of the ties, s is the spacing of the transverse reinforcement, A_s is the area of the transverse reinforcement, f_{yw} is the yield strength of the transverse reinforcement, P is the axial load on the column at shear failure, and θ is the critical crack angle from the horizontal (assumed to be 65°). For the limit state material model to work properly, the limit curve needs to be defined in units of psi or MPa.

The concrete is simulated with the nonlinear Concrete04 material in which the envelope of the compressive stress-strain response is defined using the model proposed by Mander et al. (1988). In this model, for unloading and reloading in compression, the Karsan-Jirsa model (1969) is used to determine the slope of the curve.

The tensile strength of concrete f_{cr} (compression is negative) is defined by the following expression:

$$f_{cr} = 0.33\sqrt{(-\sigma_B)} \tag{7}$$

where, σ_B concrete compressive strength (in MPa).

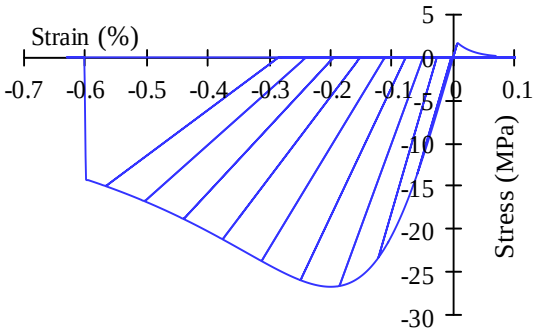

Figure 7. Concrete constitutive law (Mander et al. model)

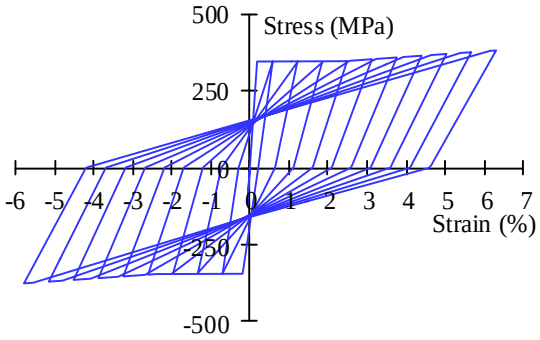

Figure 8. OpenSees hysteretic model for rebar

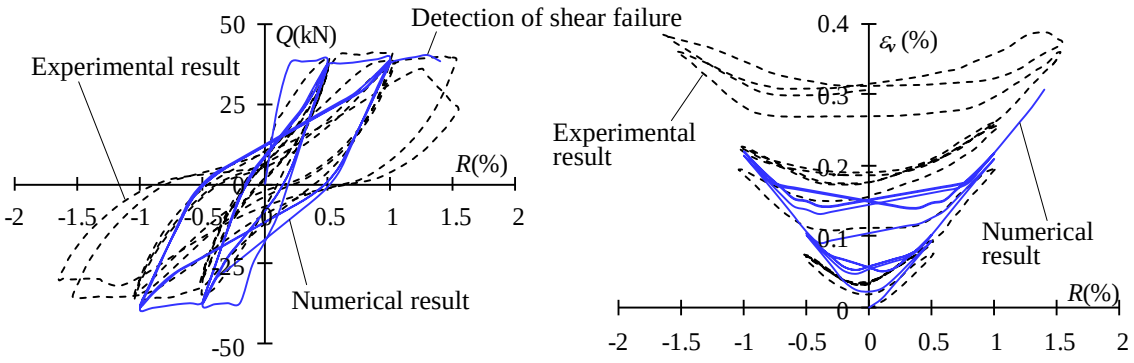

Figure 9. Comparison of experimental results and numerical results of OpenSees

For tensile loading, an exponential curve is used to define the envelope to the stress-strain curve. For unloading and reloading in tension, the secant stiffness is used to define the path. The corresponding constitutive law is illustrated in Fig. 7.

Fig. 8 shows the constitutive law of longitudinal reinforcement with tri-linear skeleton curve utilizing Hysteretic material. In the Hysteretic material model, pinching of stress and strain, damage due to ductility and energy, and degraded unloading stiffness based on ductility can be considered. In this study, damage due to ductility and energy, and degraded unloading stiffness based on ductility are considered.

Five integration points along the nonlinear beam-column element are defined. The modified Newton solution algorithm is used to solve nonlinear equations.

The cyclic analysis is carried out by imposing lateral displacements to node 3. The comparison of experimental and numerical results is shown in Fig. 9. The stress-strain relationship of a rebar at the top section (one of the critical sections) is provided in Fig. 10. The numerical result as shown in Fig. 10 indicates that the stress of rebar at the end of column has reached the yield strength. And numerical lateral capacity almost agrees with the experimental one. However, shear failure is detected when the drift ratio, R, is greater than 1.3% (see Fig. 9). Before that, the response of ε_v of numerical model

matches the experimental result closely. The detection of shear failure is related to modelling the shear spring and shear limit curve.

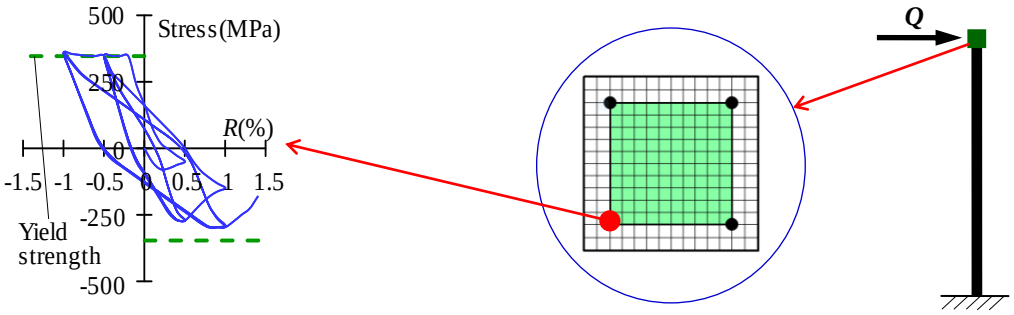

Figure 10. Numerical result of stress of longitudinal reinforcement (OpenSees)

NUMERICAL MODELLING USING VECTOR2

This section describes a nonlinear numerical study on the specimen based on VecTor2. VecTor2 is a nonlinear finite element program for the analysis of two-dimensional reinforced concrete structures and has been developed at the University of Toronto. The theoretical bases of VecTor2 are the Modified Compression Field Theory (MCFT) proposed by Vecchio FJ and Collins MP (1986) and the Disturbed Stress Field Model (DSFM) proposed by Vecchio FJ (2000). VecTor2 permits accurate assessments of structural performance (strength, post-peak behaviour, failure mode, deflections and cracking) of RC elements regardless of failure modes. The Vector2 bundle includes: FormWorks, a graphics-based preprocessor program that simplifies the model building; Augustus, a complete VecTor2 post-processor that may provide all the global and local results in useful numeric or graphic formats. It is also able to display the specimen crack pattern at each stage of imposed displacement which is very useful to detect numerical failure mode.

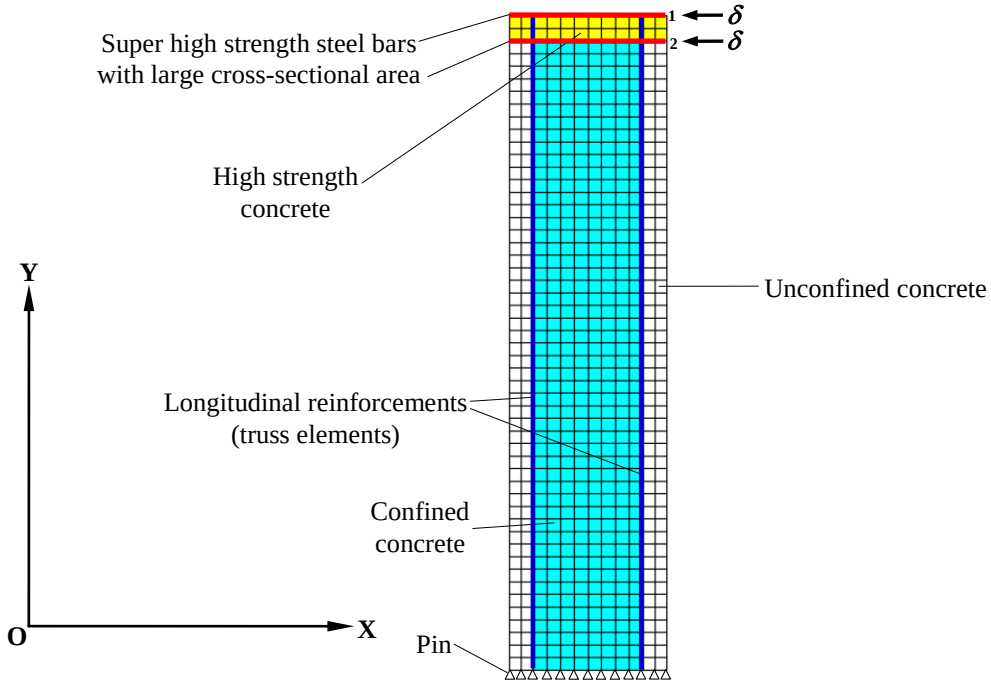

Figure 11. FormWorks model

In VecTor2, the automatic mesh generation facility with the hybrid discretization type is used to create the mesh of the specimen as shown in Fig. 11. In this model, the specimen is represented with rectangular elements for the concrete and truss bar elements for the longitudinal reinforcing bars.

Nodes at the bottom end of the column are restrained in both X and Y directions. However, all the other nodes are unconstrained. In order to constrain the rotation of upper stub and prevent localized failure where the displacement load is applied, the upper stub is modelled with high strength concrete reinforced by two super high strength steel bars with large cross-sectional area, and lateral displacements δ are applied to node 1 and node 2 simultaneously.

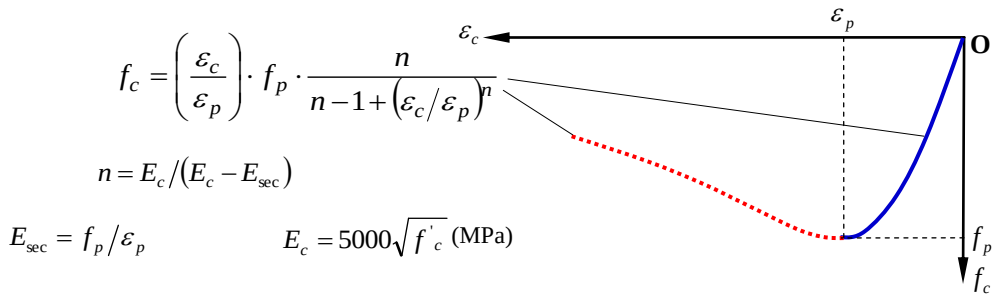

where, f_c is the principal compressive stress, ε_c is the compressive principal strain, f_p is the peak compressive stress, ε_p is the strain corresponding to f_p, and f'_c is the unconfined uniaxial concrete cylinder strength.

Figure 12. Popovics pre-peak and post-peak concrete compression response

In this study, two reinforced concrete material types are utilized for the column region. One type represents the unconfined concrete. The other type models the confined concrete. Confinement effects are taken into account by means of the geometric percentage of in-plane and out-of-plane reinforcements according to the VecTor2 & Formworks User's Manual (Wong et al., 2013) for confined concrete elements. With regard to concrete models, Popovics (Normal Strength Concrete) model is selected for the pre-peak compression response, and Popovics / Mander model is selected for the post-peak compression response which is the same equation with the Popovics (NSC) model. The details of skeleton curve for concrete compression response are shown in Fig. 12.

where, f'_{cc} is the uniaxial compressive strength, and ε_{cc} is the strain corresponding to f'_{cc}.

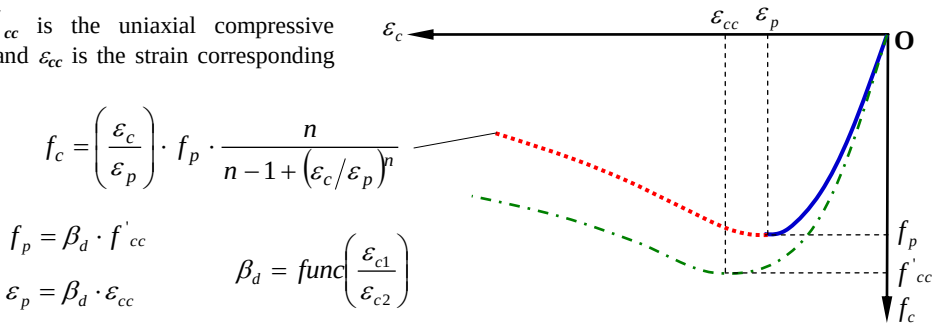

Figure 13. Strength and strain-softened compression response

$$\beta_d = \frac{1}{1+C_s \cdot C_d} \le 1 \qquad r = -\frac{\varepsilon_1}{\varepsilon_2} \le 400$$

$$C_d = \begin{cases} 0 & if \quad r < 0.28 \\ 0.35(r-0.28)^{0.8} & if \quad r > 0.28 \end{cases}$$

$$C_s = \begin{cases} 1.0 & \textit{if shear slip not considered} \\ 0.55 & \textit{if shear slip considered} \end{cases}$$

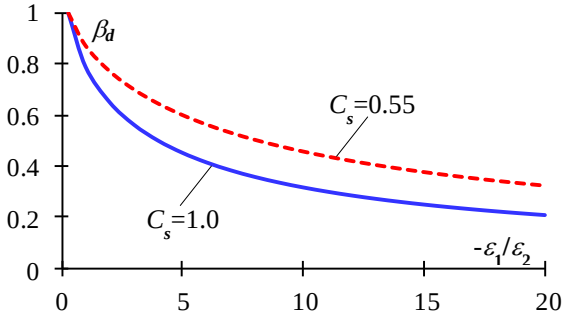

Figure 14. Compression softening parameter (Vecchio 1992-A model)

For cracked concrete subjected to a tension-compression stress state, compression softening behaviour should be considered. Compression softening in cracked concrete is the reduction of compressive strength and stiffness, relative to the uniaxial compressive strength, due to coexisting transverse cracking and tensile straining. This reduction can be substantial and have considerable

effects on the load-deformation response of reinforced concrete structures, in terms of stiffness, ultimate strength capacity and ductility. The strength-and-strain softened models, as shown in Fig. 13, use β_d to reduce both the uniaxial compressive strength, f'_{cc}, and corresponding strain, ε_{cc}, to determine the peak compressive strength, f_p, and corresponding strain, ε_p, used in the compression response models. The value of β_d is a function of $\varepsilon_1/\varepsilon_2$ - the ratio of the principal tensile strain to the principal compressive strain. In this study, Vecchio 1992-A model as shown in Fig. 14 is used to avoid overestimation of stiffening effect when the principal tensile strains are very large such as the yielding of the reinforcement.

In tension, concrete is predominantly brittle, and its response can be differentiated into uncracked and cracked response. Prior to cracking the response is assumed to be linear-elastic in VecTor2, as follows:

$$f_{c1} = E_c \cdot \varepsilon_{c1} \quad for\ 0 < \varepsilon_{c1} < \varepsilon_{cr} \tag{8}$$

$$\varepsilon_{cr} = f_{cr}/E_c \tag{9}$$

where, ε_{cr} is the cracking strain, E_c is the initial tangent stiffness of concrete, ε_{c1} is the principal tensile strain, and f_{cr} is the cracking stress of the concrete determined by the cracking criterion model.

After concrete cracks, the concrete is still effectively bonded to the reinforcement between cracks and can carry significant tensile stresses. This action is referred to as the "tension-stiffening effect". In this study, the Modified Bentz 2003 model is used for tension stiffening. The Modified Bentz 2003 formulation for tension stiffening incorporates the percentage of reinforcement as well as bond characteristics; it is the default model in VecTor2. The formulations are as follows:

$$f_{c1} = \frac{f'_t}{1+\sqrt{c_t \cdot \varepsilon_{c1}}} \quad for\ \varepsilon_{c1} \geq \varepsilon_{cr} \tag{10}$$

$$c_t = 3.6 t_d \cdot m \tag{11}$$

$$t_d = 0.6 \tag{12}$$

$$1/m = \sum_{i=1}^{n} 4\rho_i / d_{bi} \cdot \left|\cos(\theta - \alpha_i)\right| \tag{13}$$

where, ρ_i is the reinforcement ratio, d_{bi} is the rebar diameter, θ is the inclination of the principle direction, and α_i is the inclination of reinforcement.

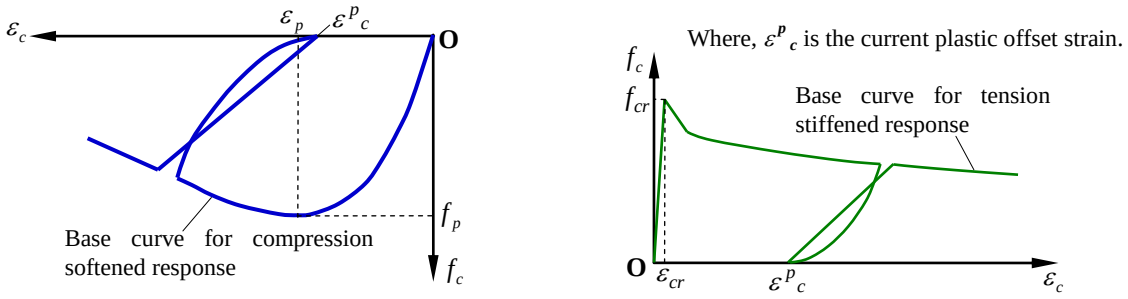

Figure 15. Palermo and Vecchio model of concrete hysteretic response in compression and tension

In plain concrete, the response of post-cracking is assumed to be linear.

For hysteretic response of concrete, nonlinear model proposed by Palermo and Vecchio (2002) is used as shown in Fig. 15. The hysteretic loops are indicative of the internal damage and energy

dissipation under cyclic loading.

For reinforcement model, ductile steel reinforcement is chosen for the reinforce type, and Menegotto-Pinto model is selected for the hysteretic response as shown in Fig. 16. This model includes the Bauschinger effect and defines an asymptotic curve tangential to two asymptotic lines at the initial (origin) and end (target) points. Perfect bond model is assumed between the bar and concrete element to prevent deformation of the bond element.

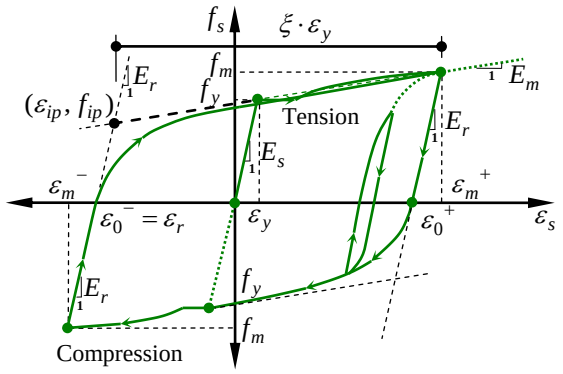

$$f_{eq} = b \cdot \varepsilon_{eq} + \frac{(1-b)\cdot \varepsilon_{eq}}{\left(1+\varepsilon_{eq}^{R}\right)^{1/R}}$$

$$f_{eq} = \frac{f_s - f_r}{f_{ip} - f_r}, \quad \varepsilon_{eq} = \frac{\varepsilon_s - \varepsilon_r}{\varepsilon_{ip} - \varepsilon_r}, \quad (\varepsilon_r = \varepsilon_0 \text{ and } f_r = 0)$$

$$b = \frac{E_m}{E_r}, \quad R = R_0 - \frac{a_1 \cdot \xi}{a_2 + \xi}, \quad \xi \cdot \varepsilon_y = \left(\varepsilon_m - \varepsilon_{ip}\right)$$

$$E_r = E_s\left(0.8 + \frac{1}{5 + 1000\varepsilon_m}\right)$$

$$f_s = f_{sj-1} + E_r\left(\varepsilon_j - \varepsilon_{j-1}\right)$$

where, f_{eq} and ε_{eq} are the normalized stress and strain, and f_{ip} and ε_{ip} are the stress and strain at the intersection point between the initial tangent at the origin and the asymptote at the target, respectively. b is the strain hardening ratio of the intended slope (E_m) at the target point to the unloading or initial reloading stiffness (E_r) at the origin. R is the independent parameter which defines the curvature according to experimental parameters, R_0, a_1, and a_2. In the VecTor2 implementation, R_0, a_1, and a_2 are taken 15, 18.5 and 0.15, respectively and the values of R are limited between 1 and 15. $\xi \cdot \varepsilon_y$ is the strain difference between the strain at the intersection point, ε_{ip} and the maximum (target) strain attained at the previous cycle, ε_m. In addition, f_m is the stress corresponding to ε_m, E_m is the tangent stiffness at ε_m, E_r is the unloading or initial reloading modulus, ε_0 is the plastic offset strain in the current cycle, f_y is yield strength corresponding to the yield strain, ε_y, and E_s is the elastic modulus of the monotonic stress-strain response.

Figure 16. Menegotto-Pinto model of ductile steel reinforcement for hysteretic response

Summation of the material properties for the concrete elements, reinforcement elements, bond elements, and the chosen analytical models for each material are shown in Table 3. Further details of the analytical parameters can be investigated in the VecTor2 & Formworks User's Manual.

Table 3. Analysis parameters of VecTor2

Convergence Criteria	Displacements - Weighted	Concrete Bond	Perfect Bond
Compression Base Curve	Popovics (NSC)	Concrete Creep / Relax	Not Considered
Compression Post-Peak	Popovics / Mander	Concrete Hysteresis	Nonlinear w/ Plastic Offsets
Compression Softening	Vecchio 1992-A	Rebar Dowel Action	Not Considered
Tension Stiffening	Modified Bentz 2003	Rebar Buckling	Not Considered
Tension Softening	Linear	Previous Load History	Considered
Concrete Dilatation	Variable - Kupfer	Slip Distortion	Walraven (Monotonic)
Cracking Criterion	Mohr-Coulomb (Stress)	Strain Rate Effects	Not Considered
Crack Stress Calculation	Basic (DSFM/MCFT)	Geometric Nonlinearity	Considered
Crack Width Check	Crack Limit (Agg/2.5)	Crack Allocation	Uniform Spacing

Based on the numerical models as mentioned above, the results from the VecTor2 are shown in Fig. 17. Fig. 18 presents the deformed shape and crack distribution of the column at drift ratios of 0.5%, 1.0%, and 1.5%, respectively. The stress of longitudinal reinforcement vs. drift angle response of a rebar at the top position of the specimen is presented in Fig. 19. The flexural stiffness based on VecTor2 almost agrees with the experimental one. This response is more accurate than the numerical result based on OpenSees, because VecTor2 considers the load-deformation behaviour of cracked reinforced concrete subjected to shear. In addition, lateral capacity of numerical results based on VecTor2 almost matches the experimental one. The changing of ε_v for numerical model leans toward the same tendency with the response of experimental one. At the drift ratio of 0.5%, many small flexural cracks and some large shear cracks developed. At the drift ratio of 1.5%, the number of large shear cracks increase significantly, the crushing of concrete elements is predicted. This demonstrates

the column fails in a shear manner. Moreover, the numerical result in Fig. 19 indicates the stress of rebar at the end of column has reached the yield strength. VecTor2 does not require assumptions on shear spring. The parameters required for modelling are mostly physical parameters. The program could successfully predict the behaviour of shear-flexural-critical column. However, modelling of a RC element with finite element in VecTor2 requires more modelling efforts and computing time than other lumped spring approaches.

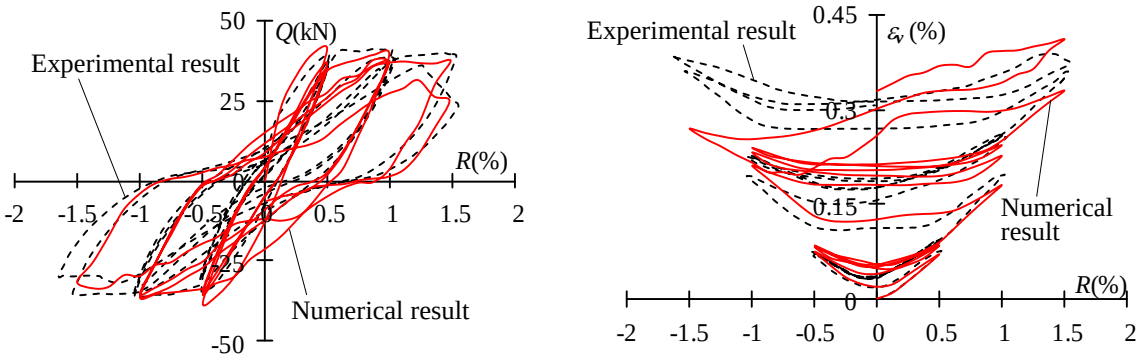

Figure 17. Comparison of experimental results and numerical results of Vector2

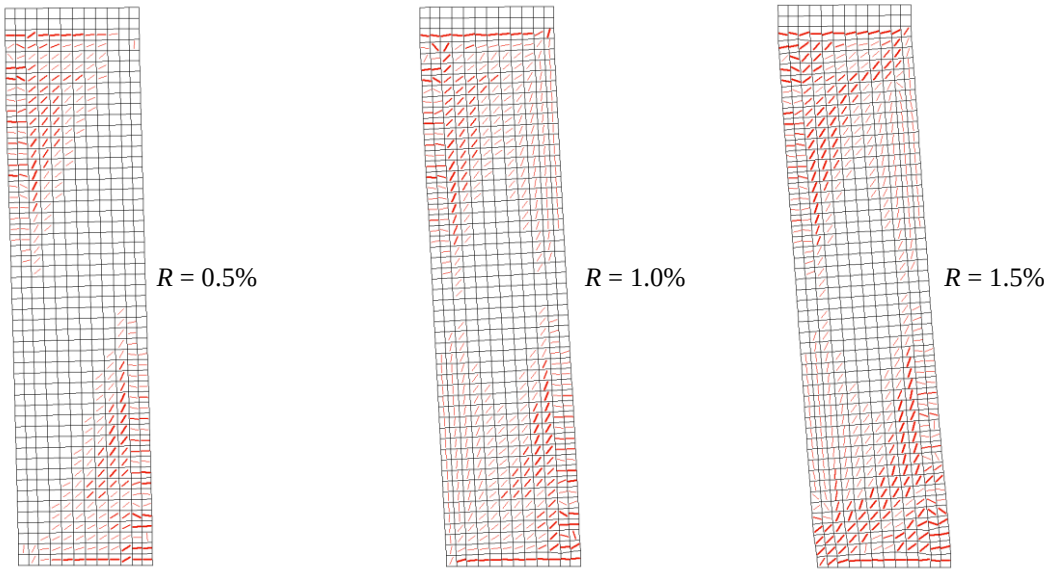

Figure 18. Combined view of displacement and crack direction in depth side by VecTor2

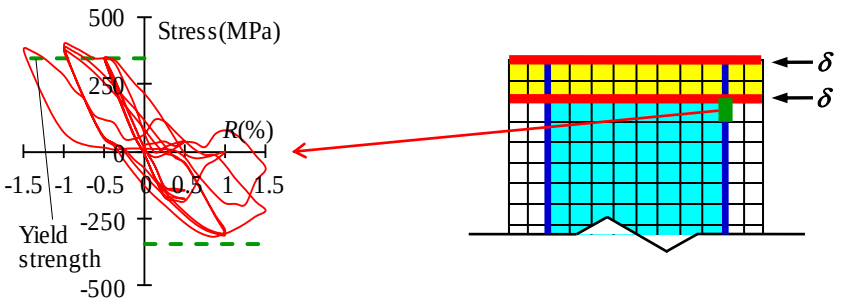

Figure 19. Numerical result of stress of longitudinal reinforcement (VecTor2)

CONCLUSIONS

The numerical studies of the tested specimen lead to the following conclusions:
(1)It is possible to detect shear failure of the specimen using OpenSees by introducing shear spring element and shear limit curve. The model with shear spring, which was empirically calibrated, is computationally efficient.
(2)The numerical results based on OpenSees almost agree with the experimental ones before detection of shear failure.
(3)The response of flexural stiffness based on VecTor2 is more accurate than the numerical result based on OpenSees because VecTor2 considers the load-deformation behaviour of cracked reinforced concrete subjected to shear. Analysis with VecTor2 model is computationally more demanding than the analysis with OpenSees. However, the modelling approach can be applied to more general configuration of geometry and reinforcement layout.

AKCNOWLEDGEMENT

The authors would like to thank Professor F.J. Vecchio at the University of Toronto for providing VecTor2 software utilized for numerical study.

REFERENCES

Li W and Esaki F (2010) "Experimental Investigation on Jointing Technique of Existing RC Column and Seismic Retrofit Steel Brace", *Architectural Institute of Japan (AIJ) Kyushu Chapter Architectural Research Meeting (Structure)*, 49(1): 553-556 (In Japanese)

Mazzoni S, McKenna F, Scott M H, Fenves GL, et al. (2007) OpenSees Command Language Manual, *The Regents of the University of California*

Vecchio FJ, Bentz EC and Collins MP (2004) "Tools for forensic analysis of concrete structures", *Computer and Concrete*, 1 (1): 1-14

Architectural Institute of Japan (1990) Ultimate Strength and Deformation Capacity Buildings in Seismic Design, AIJ (In Japanese)

Sezen H (2002) Seismic behavior and modeling of reinforced concrete building columns, Ph.D. Thesis, Department of Civil and Environmental Engineering, University of California, Berkeley, United States of America

Elwood KJ and Moehle JP (2003) Shake Table Tests and Analytical Studies on the Gravity Load Collapse of Reinforced Concrete Frames, Pacific Earthquake Engineering Research Center, University of California, Berkeley, Calif. PEER Report 2003/01

Elwood KJ and Moehle JP (2005) "Drift capacity of reinforced concrete columns with light transverse reinforcement", *Earthquake Spectra: February*, 21(1): 71-89

Mander JB, Priestley MJN and Park R (1988) "Theoretical stress-strain model for confined concrete", *Journal of Structural Engineering ASCE*, 114(8): 1804-1826

Karsan ID and Jirsa JO (1969) "Behavior of concrete under compressive loadings", *Journal of Structural Division ASCE*, 95(ST12): 2543-2563

Vecchio FJ and Collins MP (1986) "The Modified Compression Field Theory for Reinforced Concrete Elements Subject to Shear", *ACI Journal*, 83(2): 219-231

Vecchio FJ (2000) "Disturbed Stress Field Model for Reinforced Concrete: Formulation", *ASCE Journal of Structural Engineering*, 126(9): 1070-1077

Wong PS, Vecchio FJ and Trommels H (2013) VecTor2 & FormWorks User's Manual, 2nd Ed

Palermo D and Vecchio FJ (2002) Behaviour and Analysis of Reinforced Concrete Walls Subjected to Reversed Cyclic Loading, Publication No. 2002-01, Department of Civil Engineering, University of Toronto